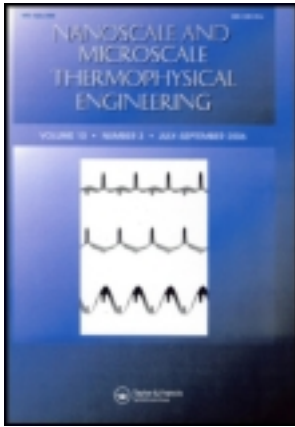


This article was downloaded by: [University of Virginia, Charlottesville]

On: 01 July 2013, At: 07:32

Publisher: Taylor & Francis

Informa Ltd Registered in England and Wales Registered Number: 1072954 Registered office: Mortimer House, 37-41 Mortimer Street, London W1T 3JH, UK



Nanoscale and Microscale Thermophysical Engineering

Publication details, including instructions for authors and subscription information:

<http://www.tandfonline.com/loi/umte20>

Impedance Matching of Atomic Thermal Interfaces Using Primitive Block Decomposition

Carlos A. Polanco^a, Christopher B. Saltonstall^b, Pamela M. Norris^b, Patrick E. Hopkins^b & Avik W. Ghosh^a

^a Department of Electrical and Computer Engineering, University of Virginia, Charlottesville, Virginia

^b Department of Mechanical and Aerospace Engineering, University of Virginia, Charlottesville, Virginia

Published online: 27 Jun 2013.

To cite this article: Carlos A. Polanco, Christopher B. Saltonstall, Pamela M. Norris, Patrick E. Hopkins & Avik W. Ghosh (2013): Impedance Matching of Atomic Thermal Interfaces Using Primitive Block Decomposition, *Nanoscale and Microscale Thermophysical Engineering*, 17:3, 263-279

To link to this article: <http://dx.doi.org/10.1080/15567265.2013.787572>

PLEASE SCROLL DOWN FOR ARTICLE

Full terms and conditions of use: <http://www.tandfonline.com/page/terms-and-conditions>

This article may be used for research, teaching, and private study purposes. Any substantial or systematic reproduction, redistribution, reselling, loan, sub-licensing, systematic supply, or distribution in any form to anyone is expressly forbidden.

The publisher does not give any warranty express or implied or make any representation that the contents will be complete or accurate or up to date. The accuracy of any instructions, formulae, and drug doses should be independently verified with primary sources. The publisher shall not be liable for any loss, actions, claims, proceedings, demand, or costs or damages whatsoever or howsoever caused arising directly or indirectly in connection with or arising out of the use of this material.

IMPEDANCE MATCHING OF ATOMIC THERMAL INTERFACES USING PRIMITIVE BLOCK DECOMPOSITION

Carlos A. Polanco¹, Christopher B. Saltonstall²,
Pamela M. Norris², Patrick E. Hopkins², and Avik W. Ghosh¹

¹Department of Electrical and Computer Engineering, University of Virginia,
Charlottesville, Virginia

²Department of Mechanical and Aerospace Engineering, University of Virginia,
Charlottesville, Virginia

We explore the physics of thermal impedance matching at the interface between two dissimilar materials by controlling the properties of a single atomic mass or bond. The maximum thermal current is transmitted between the materials when we are able to decompose the entire heterostructure solely in terms of primitive building blocks of the individual materials. Using this approach, we show that the minimum interfacial thermal resistance arises when the interfacial atomic mass is the arithmetic mean, whereas the interfacial spring constant is the harmonic mean of its neighbors. The contact-induced broadening matrix for the local vibronic spectrum, obtained from the self-energy matrices, generalizes the concept of acoustic impedance to the nonlinear phonon dispersion or the short-wavelength (atomic) limit.

KEY WORDS: Phonon transport, Phonon NEGF, atomic interfaces, interfacial forces, adhesion

INTRODUCTION

Today's experimental techniques are opening up the possibility of tuning thermal conductivity of materials by engineering their thermal impedance at the nanoscale [1]. At these characteristic lengths (~ 10 nm), thermal boundary conductance (TBC) of interfaces provides a major contribution to the thermal conductance of the system, making understanding of impedance matching at interfaces critical. Several experiments [2–9] and simulations [10–15] have already shown the dependence of TBC with interfacial impurities, mixing, defects, chemistry, or bond strength. Nevertheless, the standard models to calculate TBC, the acoustic mismatch model [16] and the diffuse mismatch model [17], completely neglect the properties of the interface. Although some work has been done to include those properties in a model [9, 18–21], proper identification of the key physics determining TBC

Manuscript received 12 December 2012; 15 March 2013.

C.A.P. thanks Professor Peter Arnold and Dr. John Duda for the useful discussions. C.A.P. and A.W.G. are grateful for the support from NSF-CAREER (QMHP 1028883). C.A.P., A.W.G., and P.E.H. are greatly appreciative for the funding from NSF-IDR (CBET 1134311). P.E.H. is thankful for the funding from the LDRD program office at Sandia National Laboratories.

Address correspondence to Carlos A. Polanco, Department of Electrical and Computer Engineering, University of Virginia, 351 McCormick Rd., Charlottesville, VA, 22904-4743. E-mail: cap3fe@virginia.edu

NOMENCLATURE

A	normalized displacement amplitude, $1/kg^{1/2}$	t	time
a	atomic spacing	t_1, t_2	frequency-dependent force constant
B	normalized displacement amplitude, $1/kg^{1/2}$	u_n	normalized displacement of n th atom, $1/kg^{1/2}$
C	normalized displacement amplitude, $1/kg^{1/2}$	v_g	group velocity
\hbar	Planck's constant	Z	acoustic impedance
I	thermal current	Greek symbols	
J	thermal current, W	Γ	broadening matrix
k	force constant	ϵ_1, ϵ_2	frequency-dependent mass
L	length of the interface	λ	wavelength
m	atomic mass	ρ	mass density
N	number of atoms	ω	frequency
N_b	number of blocks at the interface	ω_c	cutoff frequency
N_1, N_2	Bose-Einstein distributions	Subscripts	
q	wave vector	hm	half-mass
R	phonon reflection coefficient	hs	half-spring
T	phonon transmission coefficient	n	atom label in the chain

is still incomplete, but it is crucial for impedance matching design at the nanoscale. This will lead the emerging field of phonon engineering to follow the successful steps of electronics and photonics, where engineering of nanoscale properties has endowed the fields with high degrees of tunability.

Phonon transport across an interface is a convoluted process that involves the differing phonon modes, the short coherence lengths of the quantized vibrations, and their broadband transport properties. In addition, it involves complex and diverse interfacial atomic structures that depend strongly on materials and fabrication protocols. To account for the many factors affecting phonon flow across interfaces, we use the term *thermal impedance* to generalize the concept of acoustic impedance and include the contributions to phonon flow from the whole frequency spectrum, atomistic details at the junctions, tensorial properties of materials, and coherent and incoherent scattering.

Though the overall goal of our study is to explore the physics of thermal impedance matching at interfaces covering the entire gamut from 1D to 3D, from linear to nonlinear dispersion and from coherent transport—that is, when phonons do not suffer phase-breaking scattering processes and therefore interference patterns arise—to incoherent or phase-breaking transport, we will start building our intuition by studying coherent thermal impedance matching between two dissimilar 1D materials by controlling the properties of a single mass (Figure 1a) or spring (Figure 1b) in between. This toy model presents a starting point to understand ballistic contributions to TBC by important factors already identified in the literature, such as interfacial impurities, mixing, defects, chemistry, or bond strength [2–6, 8, 9, 19]. In fact, some authors have used this toy model to support their molecular dynamic simulation results, arguing that TBC increases with increased bond strength [10, 11, 14].

The results for coherent 1D thermal impedance matching are incredibly diverse. For example, to achieve maximum thermal conductance we want the interfacial impedance to

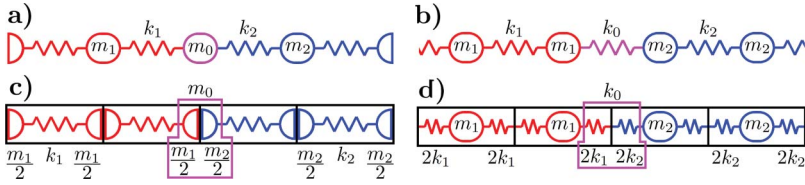


Figure 1 (a) 1D interface between dissimilar materials with an arbitrary atom in between. (b) Interface with an arbitrary bond in between. (c) Optimal coupling between the contacts happens when we can describe the entire heterostructure only in terms of building blocks of individual materials. This decomposition makes the optimal atomic mass the arithmetic mean of its neighbors $m_0 = m_1/2 + m_2/2$. (d) Maximum thermal conductance occurs when the interfacial spring constant is the harmonic mean of its neighbors $1/k_0 = 1/2k_1 + 1/2k_2$ (recall that a spring half as short is twice as strong), which follows again from a decomposition in terms of blocks of individual materials (color figure available online).

maximize the area under the transmission function, like a *broadband* filter. Following this criterion, we point out that the best matching interfacial mass (m_0) for the single mass junction (Figure 1a) is the *arithmetic* mean between the masses of the contacts [22]. For a single spring junction (Figure 1b), Zhang et al. [20] found that the best matching interfacial spring constant (k_0) is the *harmonic* mean between the contact springs. When the goal is to achieve maximum phonon transmission around a fixed frequency, our expectations based on our knowledge of optical antireflection coatings posit that unity phonon transmission would require a quarter-wave plate with an impedance equal to the geometric mean of its neighbors. In view of these diverse results, our aim here is to put these averages on a common footing and motivate them qualitatively in terms of the intrinsic physical properties of the junction itself.

The central point of this article is that the degree of mismatch at a single atom or bond interface depends on our ability to express the entire heterostructure solely in terms of primitive building blocks on either side. For instance, we find that the optimal mass (Figure 1a) is one that can be decomposed precisely into two half-masses arising from the materials on either side (Figure 1c). This decomposition makes the optimal mass the *arithmetic* mean of its neighbors; that is, $m_0 = m_1/2 + m_2/2$. For an analogous decomposition of the spring constant (Figures 1b and 1d), we find that the optimal spring constant equals the *harmonic* mean of its neighbors; that is, $1/k_0 = 1/2k_1 + 1/2k_2$ (recall that springs in series add like resistances in parallel). Any deviation from those optimal decompositions (optimally coupled interfaces, OCIs) adds an extra barrier for heat carriers reducing the interfacial transmission.

The thermal conductance for OCIs is characterized by the contact-induced broadening matrix $\Gamma(\omega)$ extracted from the local vibronic spectrum, which generalizes the concept of acoustic impedance (Z). Γ not only includes nonlinear dispersion and short-wavelength (atomic) limit effects, but its matrix character can account for the different modes or channels available for transport when higher dimensions are considered. In addition, this character can include intricate chemical details at the interface, which may greatly affect the transport process as shown recently by Losego et al. [23]. It is worth emphasizing that Γ alone is not enough to correctly represent general phonon transport. The broadening's Hilbert transform must also be included in the Green's function to properly account for the sum rule of the local density of states [24].

This generalization not only relates the continuum formalism [25] with the discrete nonequilibrium Green's functions (NEGF) formalism [24, 26–29] but also provides a way to extrapolate known results based on acoustic impedance to OCI. For instance, we can totally eliminate the interfacial reflection by impedance matching of the Γ matrices (more

precisely, the projected self-energies, Σ), realized when Γ for the central layer equals the geometric mean of its neighbors. The generalization may also allow us to use existing techniques from other engineering fields in phonon engineering. For instance, broadband filtering techniques from microwave engineering may be useful to engineer interfaces with maximum thermal conductance.

This article begins by explaining the idea of splitting 1D chains into primitive blocks, which define the properties of contacts or semi-infinite chains. Then, using the block concept, phonon transmission is calculated, and it is also shown that maximum thermal conductance occurs when the entire heterostructure can be expressed solely in terms of the building blocks on either side of the interface. These types of interfaces (OCI) are then studied and characterized and it is shown that OCI generalizes an abrupt interface in the continuum limit with Γ generalizing Z .

BLOCK PARTITION OF 1D CHAIN AND CONTACTS

An infinite 1D chain of masses coupled by springs (Figure 2a) can be decomposed into different arrays of primitive blocks (Figures 2b and 2c). According to the blocks, different contacts—that is, semi-infinite chains—can be built from the same homogeneous material. As we will also show, we can equally view a chain of half-spring blocks as a virtual chain of half-mass blocks, provided that the corresponding mass and spring constant are *frequency dependent*.

Consider a 1D infinite chain of masses m_1 , separated by a distance a and connected by springs with force constant k_1 (Figure 2a). Newton's equation for the normalized displacement of the n^{th} atom, $\mu_n(t) = u_n e^{-i\omega t}$ with dimensions inverse square root of mass—that is, $[\mu] = [M^{-1/2}]$ —is given by

$$\omega^2 m_1 u_n = -k_1 u_{n-1} + 2k_1 u_n - k_1 u_{n+1}. \quad (1)$$

Plane waves $u_n = A e^{iq_1 n a}$ solve this set of periodic equations. In addition, after their substitution in Eq. (1) we obtain the dispersion relation

$$\omega^2 m_1 = 2k_1 - 2k_1 \cos(q_1 a), \quad (2)$$

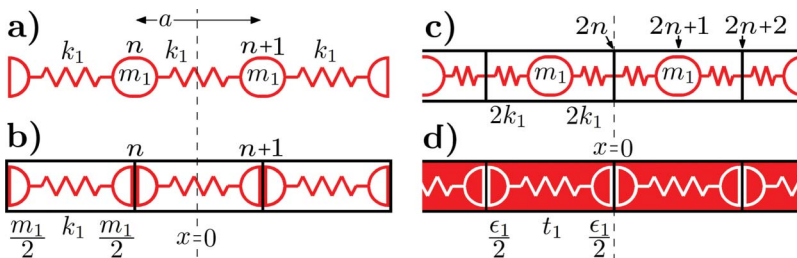


Figure 2 (a) 1D infinite chain of masses m_1 , separated by a , joined by springs with force constant k_1 . (b) and (c) Same chain separated into different blocks whose boundaries define different contacts. (b) Partition into half-mass blocks with half masses across the boundary. (c) Partition into half-spring blocks with half springs across the boundary. (d) The half-spring blocks can be reinterpreted as half-mass blocks, provided that the corresponding mass and spring constant are frequency dependent. The non-white background of the blocks represents this dependence (color figure available online).

which is more commonly written as [30]

$$\omega = 2\sqrt{\frac{k_1}{m_1}} \left| \sin\left(\frac{q_1 a}{2}\right) \right|. \quad (3)$$

Splitting each mass into its series equivalent $m_1 = m_1/2 + m_1/2$, the chain can be partitioned into blocks with boundaries at the *masses*; that is, half-mass blocks (Figure 2b). In this case, Eqs. (1) and (2) can be reorganized to reflect the partition as

$$\omega^2 \left(\frac{m_1}{2} + \frac{m_1}{2} \right) u_n = -k_1 u_{n-1} + 2k_1 u_n - k_1 u_{n+1} \quad (4)$$

$$\omega^2 \left(\frac{m_1}{2} + \frac{m_1}{2} \right) = 2k_1 - 2k_1 \cos(q_1 a). \quad (5)$$

Note that the plane waves solving those equations represent $|A|^2 N m_1$ propagating phonons of energy $\hbar\omega$ (N is the number of atoms in the chain) and carry a thermal current given by [27]

$$J = \hbar k_1 \sin(q_1 a) |A|^2 = \hbar \frac{\Gamma_1^{hm}}{2} |A|^2 = \hbar \omega \frac{m_1}{a} v_g(\omega) |A|^2, \quad (6)$$

where

$$\Gamma_1^{hm} = 2k_1 \sin(q_1 a) \quad (7)$$

(‘*hm*’ stands for half-mass) is the non-zero entry of the broadening matrix used in NEGF formalism and $v_g(\omega)$ is the frequency-dependent phonon group velocity.

Similarly, we can split each spring into its series equivalent $1/k_1 = 1/2k_1 + 1/2k_1$, separating the chain (Figure 2a) into blocks with boundaries at the *springs*; that is, half-spring blocks (Figure 2c). The latter system is described by

$$\omega^2 m_1 u_{2n+1} = -2k_1 u_{2n} + 2(k_1 + k_1) u_{2n+1} - 2k_1 u_{2n+2}, \quad (8)$$

$$0 = -2k_1 u_{2n-1} + 2(k_1 + k_1) u_{2n} - 2k_1 u_{2n+1}. \quad (9)$$

Solving for u_{2n} from Eq. (9) and for u_{2n+2} from Eq. (8) substituting n by $n + 1$ and replacing those solutions into Eq. (8) yields Eq. (1). More interestingly, solving for u_{2n+1} from Eq. (8) and for u_{2n-1} from Eq. (8) (substituting n by $n - 1$) and replacing into Eq. (9), results in an equation similar to Eq. (4)

$$\omega^2 \left(\frac{\epsilon_1}{2} + \frac{\epsilon_1}{2} \right) u_{2n} = -t_1 u_{2n-2} + 2t_1 u_{2n} - t_1 u_{2n+2}, \quad (10)$$

where

$$\epsilon_1 = \frac{m_1}{1 - \frac{\omega^2}{\omega_{c1}^2}}, \quad t_1 = \frac{k_1}{1 - \frac{\omega^2}{\omega_{c1}^2}}$$

are *frequency-dependent coefficients* and the cutoff frequency is given by $\omega_{c1} = 2\sqrt{k_1/m_1}$. In other words, the half-spring block chain can be interpreted as a virtual half-mass block chain having frequency-dependent masses and springs.

This analogy permits the extrapolation of algebraic treatments, like NEGF, from half-mass block to virtual half-mass block chains. For instance, plane waves describing the displacement at the boundaries of half-spring blocks $u_{2n} = Ae^{iq_1 2n \frac{a}{2}} = Ae^{iq_1 na}$ satisfy the dispersion relation

$$\omega^2 \left(\frac{\epsilon_1}{2} + \frac{\epsilon_1}{2} \right) = 2t_1 - 2t_1 \cos(q_1 a) \quad (11)$$

and carry a thermal current

$$J = \hbar t_1 \sin(q_1 a) |A|^2 = \hbar \frac{\Gamma^{hs}}{2} |A|^2 = \hbar \omega \frac{\epsilon_1}{a} v_g(\omega) |A|^2 \quad (12)$$

with

$$\Gamma_1^{hs} = 2t_1 \sin(q_1 a) \quad (13)$$

(‘*hs*’ stands for half-spring) the non-zero entry of the broadening matrix used in NEGF formalism for the virtual chain.

Although the same infinite chain or bulk material can be built from any block, different contacts are created from different blocks. Indeed, the block choice defines the edge of the contact, the positions in space described by displacement plane waves Ae^{iqna} (block boundaries) and, more important, the thermal current carried by those waves. One striking example of the difference between half-mass and half-spring contacts arises when we connect them together. A phonon impinging on such an interface has non-zero probability of reflection, unlike a phonon propagating in a single block chain. Note that this interface mimics a growth defect in a 1D crystal.

TRANSMISSION USING BLOCKS

Because a set of phonons of equal energy propagating in a crystal is well represented by plane waves, the transmission probability of phonons impinging at an interface can be calculated from the ratio between the thermal currents carried by the transmitted and incident waves. This section presents phonon transmission calculations using the block concept to simplify the process. It is shown that maximum transmission at every frequency, and therefore maximum thermal conductance, occurs when the entire heterostructure can be expressed solely in terms of building blocks on either side. This idea is equivalent to choosing the interfacial atomic mass as the arithmetic mean or the interfacial spring constant as the harmonic mean of its neighbors.

Interface with Mass Junction

Imagine chopping the materials of Figure 1a into half-mass blocks and the interfacial mass into a series equivalent that completes the contacts’ blocks plus some residual mass m_i ; that is,

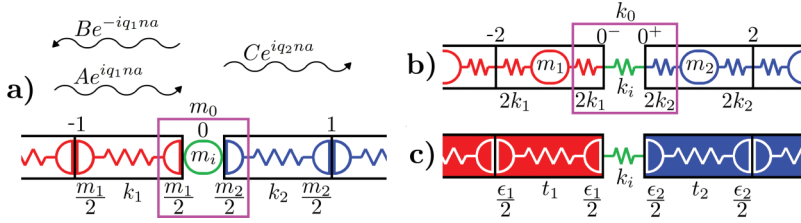


Figure 3 Decomposition of interfaces into blocks for transmission calculations. An upper bound for transmission occurs when the impurity atom m_i or bond $1/k_i$ is zero. (a) Atom junction interface split into half-mass blocks. (b) Bond junction interface split into half-spring or (c) virtual half-mass blocks. In this case, $u_{2n} = Ae^{iq_1na} + Be^{iq_1na}$ (color figure available online).

$$m_0 = \frac{m_1}{2} + m_i + \frac{m_2}{2} \tag{14}$$

(Figure 3a). Assuming incident, reflected, and transmitted plane wave solutions, transmission is given by the ratio of transmitted over incident thermal currents

$$T = \frac{J_t}{J_i} = \frac{\Gamma_2^{hm}}{\Gamma_1^{hm}} \left| \frac{C}{A} \right|^2.$$

The relationship between A and C is found by substituting the assumed solution

$$u_n = \begin{cases} Ae^{iq_1na} + Be^{-iq_1na} & n \leq 0 \\ Ce^{iq_2na} & n \geq 0 \end{cases} \tag{15}$$

into Newton’s equation at the interface of Figure 3a ($n = 0$)

$$\omega^2 \left(\frac{m_1}{2} + m_i + \frac{m_2}{2} \right) u_0 = -k_1 u_{-1} + (k_1 + k_2) u_0 - k_2 u_1. \tag{16}$$

This process is simplified using Eq. (5), noting that the real part of the right-hand side of Eq. (16) exactly cancels $\omega^2(m_1 + m_2)u_0/2$, which yields

$$\omega^2 m_i u_0 = i(A - B) \frac{\Gamma_1^{hm}}{2} - iC \frac{\Gamma_2^{hm}}{2}. \tag{17}$$

Combining this result with the fact that $u_0 = A + B = C$, the transmission T is found to be a Breit-Wigner form

$$T(\omega, m_i) = \frac{4\Gamma_1^{hm}\Gamma_2^{hm}}{4\omega^4 m_i^2 + (\Gamma_1^{hm} + \Gamma_2^{hm})^2}, \tag{18}$$

with m_i being the deviation of the interfacial mass m_0 from the arithmetic mean between the contact masses (Eq. (14)).

Note that the largest possible transmission for every ω is obtained when $m_i = 0$. This choice maximizes the thermal current flowing across the interface and the thermal conductance of the system. That is,

$$\begin{aligned}
 I_0 &= \int d\omega \frac{\hbar\omega}{2\pi} T(\omega, 0)(N_1 - N_2) \\
 &\geq \int d\omega \frac{\hbar\omega}{2\pi} T(\omega, m_i)(N_1 - N_2) = I_{m_i}.
 \end{aligned}$$

In this particular case, the system becomes equivalent to an abrupt interface between contacts built with half-mass blocks, which is referred as an OCI. When $m_i \neq 0$, transmission decreases (for all ω) so m_i can be associated with an extra barrier lowering the thermal conductance. Specifically, a delta scattering center like a single point impurity or defect at the interface.

Interface with Spring Junction

Imagine now chopping the contacts of Figure 1b into half-spring blocks and the interfacial spring into its series equivalent

$$\frac{1}{k_0} = \frac{1}{2k_1} + \frac{1}{k_i} + \frac{1}{2k_2} \quad (19)$$

(Figure 3b). Assuming incident, reflected, and transmitted plane wave solutions at the blocks' boundaries, transmission is given by the ratio of transmitted over incident thermal currents

$$T = \frac{J_t}{J_i} = \frac{\Gamma_2^{hs}}{\Gamma_1^{hs}} \left| \frac{C}{A} \right|^2.$$

The relationship between A and C is found by substituting the assumed solution

$$u_{2n} = \begin{cases} Ae^{iq_1na} + Be^{-iq_1na} & n < 0 \text{ and } n = 0^- \\ Ce^{iq_2na} & n > 0 \text{ and } n = 0^+ \end{cases} \quad (20)$$

into Newton's equation at the interface ($n = 0^-$ and $n = 0^+$) for the virtual chain (Figure 3c)

$$\omega^2 \frac{\epsilon_1}{2} u_{0^-} = -t_1 u_{-2} + (t_1 + k_i) u_{0^-} - k_i u_{0^+} \quad (21)$$

$$\omega^2 \frac{\epsilon_2}{2} u_{0^+} = -k_i u_{0^-} + (k_i + t_2) u_{0^+} - t_2 u_2. \quad (22)$$

This process is simplified using Eq. (11), noting that the real part of $t_1(u_{0^-} - u_{-2})$ from Eq. (21) and $t_2(u_{0^+} - u_2)$ from Eq. (22) exactly cancel $\omega^2 \epsilon_1 u_{0^-} / 2$ and $\omega^2 \epsilon_2 u_{0^+} / 2$, respectively, which yields

$$0 = k_i u_{0^-} - k_i u_{0^+} + i(A - B) \frac{\Gamma_1^{hs}}{2} \quad (23)$$

and

$$0 = -k_i u_{0-} + k_i u_{0+} - iC \frac{\Gamma_2^{hs}}{2}. \quad (24)$$

Combining these two results with $u_{0-} = A + B$ and $u_{0+} = C$, the transmission T is given by

$$T(\omega, k_i^{-1}) = \frac{4\Gamma_1^{hs}\Gamma_2^{hs}}{\frac{1}{4k_i^2} (\Gamma_1^{hs}\Gamma_2^{hs})^2 + (\Gamma_1^{hs} + \Gamma_2^{hs})^2}, \quad (25)$$

with k_i^{-1} measuring the deviation of the interfacial spring k_0 from the harmonic mean between the contact springs (Eq. (19)).

Note that the largest possible transmission for every ω is obtained when $k_i^{-1} = 0$. This choice maximizes the thermal current flowing across the interface and the thermal conductance of the system. In that case, the system also becomes equivalent to an abrupt interface between contacts built with half-spring blocks, which is also referred as an OCI. When $k_i^{-1} \neq 0$, transmission (for all ω) and thermal conductance decrease, so that k_i^{-1} can be associated with an extra barrier at the interface.

OPTIMALLY COUPLED INTERFACES

An OCI is an abrupt interface between half-mass or half-spring block contacts, which was proven equivalent to the single atomic or bonding interface with maximum possible transmission or thermal conductance. This section shows that an OCI can be thought of as a step barrier for phonons responsible for the scattering due to a change in propagation medium. On the other hand, a non-OCI is represented by the same step barrier plus an extra barrier caused by a deviation from the optimal case ($m_i \neq 0$ or $k_i^{-1} \neq 0$). The extra barrier decreases thermal conductance and can be associated with additional scattering mechanisms at the interface, such as impurities, mixing, or dislocations. This section presents a useful way to visualize transmission in OCI from the contact broadenings and extends the concept of OCI to abrupt junctions between contacts built with different types of blocks.

This section also shows that OCI generalizes an abrupt interface in the continuum limit without the long wavelength constraint. Moreover, the *bulk* property Z (acoustic impedance) is generalized by the *contact* property Γ (broadening), which, unlike Z , includes the atomistic details of the contact's edge and the nonlinear effects of phonon dispersion. This analogy shows a way to extrapolate previous results for interfaces in the continuum limit to the discrete limit by replacing abrupt interfaces with OCI and Z with Γ . For instance, the result of a thermal antireflection coating for a quarter-wave length plate is obtained when the plate broadening equals the geometric mean of the individual contact broadenings.

Continuous vs. Discrete Limit

The continuous medium approximation assumes that the wavelengths of interest are large enough ($\lambda \gg a$) so that the atomistic details of the media are ignorable, the dispersion is linear, and the group velocity is constant. Within this approximation, the scattering problem at an interface (Table 1, row a) is solved by assuming incident, reflected, and

Table 1 Parallel between an abrupt interface in the continuum limit and an OCI. The resemblance suggests that the contact-induced broadening matrix Γ generalizes the concept of acoustic impedance (Z) to the nonlinear phonon dispersion as well as the short-wavelength (atomic) limit. For Z , $\rho = m/a$. For Γ , $\rho = m/a$ or $\rho = \epsilon/a$ according to the block choice. Note that the matrix character of Γ can account for all of the conduction modes available in higher dimensions, for interactions beyond first neighbor and for tensorial properties of materials

Continuous	Discrete
	
b Acoustic impedance $Z = \rho v_g$	Broadening $\Gamma(\omega) = 2\omega\rho(\omega)v_g(\omega)$
c From boundary conditions $A + B = C$ $Z_1(A - B) = Z_2C$	$A + B = C$ $\Gamma_1(A - B) = \Gamma_2C$
d Energy current $J_A \propto Z A ^2$	$J_A \propto \Gamma A ^2$
e Transmission $T = \frac{4Z_1Z_2}{(Z_1+Z_2)^2}$	$T = \frac{4\Gamma_1\Gamma_2}{(\Gamma_1+\Gamma_2)^2}$

transmitted plane wave solutions and imposing boundary conditions on them to guarantee the validity of the wave equation at the interface. These conditions are nicely simplified by introducing the concept of acoustic impedance (Table 1, rows b and c [25])

$$Z = \rho v_g = \frac{m}{a} \left(a \sqrt{\frac{k}{m}} \right) = \sqrt{km}. \quad (26)$$

From them, the ratio of the wave amplitudes is calculated and then transmission is found from the ratio of transmitted over incident energy currents (Table 1, row e). Scattering at these interfaces can be connected with *medium* mismatch using the reflection coefficient

$$R = 1 - T = \left(\frac{Z_1 - Z_2}{Z_1 + Z_2} \right)^2, \quad (27)$$

which vanishes only when $Z_1|A|^2 = Z_2|A|^2$. In other words, if plane waves of the same amplitude do not carry the same energy current in both *media*, then some energy has to be reflected. That is, the scattering is solely caused by mismatch of the medium properties.

When the long wavelength constraint is relaxed, the frequency-dependent group velocity, the cutoff frequency, and the atomistic details of the interface affect the transmission (all included in calculations in the previous section). Nevertheless, particularizing the transmission calculation in section III to the optimal case ($m_i = 0$ for mass junction and $k_i^{-1} = 0$ for spring junction) displays the resemblance between an OCI and an abrupt interface in the continuum limit (Table 1). This suggests that OCI generalizes the continuous interface with Γ playing the role of acoustic impedance Z . Note that in the long wavelength limit $\Gamma \rightarrow 2\omega Z$ (for both Γ^{hm} and Γ^{hs}) and we recover the transmission result in terms of Z

$$T = \frac{4\Gamma_1\Gamma_2}{(\Gamma_1 + \Gamma_2)^2} \xrightarrow{\lambda \gg \alpha} \frac{4Z_1Z_2}{(Z_1 + Z_2)^2}. \tag{28}$$

Similar to the continuum limit, scattering in OCI is solely due to *contact* mismatch. That is, if plane waves of the same amplitude do not carry the same energy current in both *contacts* then some energy has to be reflected. The subtle difference from *medium* to *contact* reflects the fact that unlike Z , Γ is a *contact* property that ultimately depends on the block choice and carries information about the contact’s edge.

After identifying contact mismatch scattering with the transmission functional defining OCI (Table 1, row e), the extra term decreasing the transmission in Eq. (18) or (25) is associated with an additional source of scattering at the interface. Following this train of thought, an OCI is represented by a *frequency-dependent* step barrier for phonons responsible for contact mismatch scattering, whereas a non-OCI is represented by the same step barrier plus an extra barrier that decreases transmission and can be associated with impurities, mixing, or dislocations (Figure 4).

Note that if the blocks do not have a two-fold rotation symmetry around their centers—for example, the masses in a half-mass block are not equal but still their equivalent mass equals m_1 —the simplifications in Table 1, row c, are not possible for every ω . That is, abrupt interfaces between contacts built with nonsymmetric blocks do not resemble the equations in the continuum limit.

Characteristics of OCI

OCI transmission can be visualized from the contact broadenings using the reflection coefficient

$$R = 1 - T = \left| \frac{\Gamma_1 - \Gamma_2}{\Gamma_1 + \Gamma_2} \right|^2. \tag{29}$$

Unity transmission ($T(\omega_*) = 1$) is obtained when Γ s match ($\Gamma_1(\omega_*) = \Gamma_2(\omega_*)$) at a particular frequency ω_* . That is, a phonon with energy $\hbar\omega_*$ does not see the interface. Null transmission ($T(\omega) = 0$) is obtained if any of the Γ s becomes 0 or imaginary. This defines a cutoff frequency ω_c over which phonons do not propagate in the contact. In addition, note

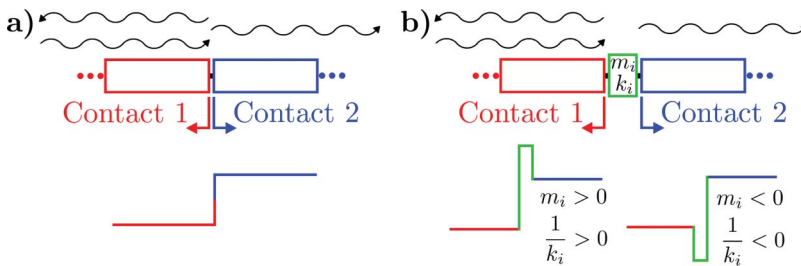


Figure 4 (a) OCI and its representation as a single barrier for phonons, which is responsible for the scattering due to propagating waves changing medium. (b) Non-OCI and its representation as a step barrier plus an extra barrier caused by a deviation from the optimal case. This extra barrier decreases thermal conductance and can be associated with impurities, mixing, or defects at the interface (color figure available online).

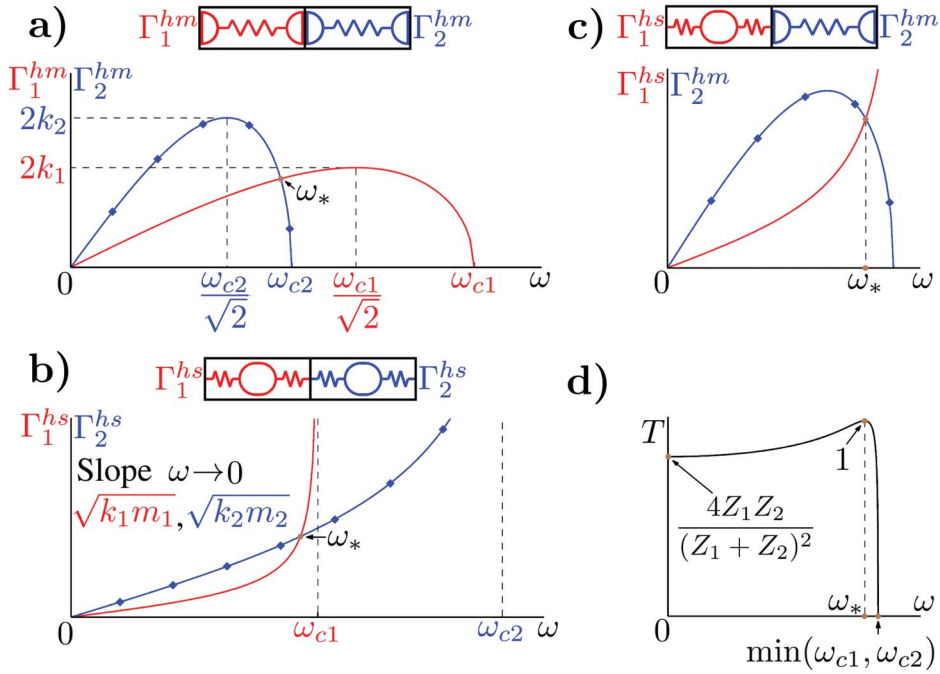


Figure 5 Transmission of OCI visualized from the broadening of the contacts (Γ_1 and Γ_2). (a), (b), and (c) Γ s for half-mass contacts, half-spring contacts, and half-spring, half-mass contacts, respectively. The dotted lines represent Γ_2 . (d) Characteristic transmission function for all previous cases. At the particular frequency ω_* , where Γ s intersect each other, transmission becomes unity and the materials match (color figure available online).

that the frequency dependence of Γ disallows the possibility of matching different contacts at every ω , making scattering unavoidable.

When a contact is built with *half-mass blocks*, Γ_1^{hm} from Eq. (7) can be rewritten using the dispersion relation as

$$\Gamma_1^{hm} = 2k_1 \sqrt{1 - \left(1 - \frac{2\omega^2}{\omega_{c1}^2}\right)^2} \quad (30)$$

with $\omega_{c1} = 2\sqrt{k_1/m_1}$. This concave function vanishes at $\omega = 0$ and $\omega = \omega_{c1}$ and has a maximum value $2k_1$ at frequency $\omega_{c1}/\sqrt{2}$ (Figure 5a). With this function in mind, transmission of an OCI between half-mass block contacts (Figure 5d) can be visualized from a plot of the real part of both contact broadenings (Figure 5a) and Eq. (29). Figures 5a and 5d show the case when the contacts match at a particular frequency ω_* ; that is, when $T(\omega_*) = 1$. This is only possible if Γ s intersect, which requires $k_1 < k_2$ and $\omega_{c1} > \omega_{c2}$ or $k_1 > k_2$ and $\omega_{c1} < \omega_{c2}$. The intersection frequency ω_* is found by equating $\Gamma_1(\omega_*) = \Gamma_2(\omega_*)$ as

$$\omega_*^2 = \begin{cases} \frac{4(m_1 k_1 - m_2 k_2)}{m_1^2 - m_2^2} & \text{if } m_1 \neq m_2 \\ [0, \min(\omega_{c1}, \omega_{c2})] & \text{if } m_1 = m_2 \text{ and } k_1 = k_2 \\ \text{never} & \text{if } m_1 = m_2 \text{ and } k_1 \neq k_2 \end{cases}$$

Note that when acoustic impedances match the intersection frequency is zero, which makes sense because in the continuous regime any wave looks like a zero frequency wave. When the contacts do not match or Γ 's never intersect, the transmission never reaches unity. This occurs if $k_1 > k_2$ and $\omega_{c1} > \omega_{c2}$ or $k_1 < k_2$ and $\omega_{c1} < \omega_{c2}$. Another interesting case occurs when the cutoff frequencies are equal, which makes $\Gamma_1 \propto \Gamma_2$ and therefore transmission is constant.

When a contact is built with *half-springs blocks*, Γ_1^{hs} from Eq. (13) can be rewritten using the dispersion relation as

$$\Gamma_1^{hs} = 4k_1 \sqrt{\frac{\omega^2}{\omega_{c1}^2 - \omega^2}}. \tag{31}$$

This convex function vanishes at $\omega = 0$, is ∞ at $\omega = \omega_{c1}$, and has a slope at $\omega = 0$ of $2\sqrt{k_1 m_1}$ (Figure 5b). Similar to the former case, Figure 5b and 5d show the case when the contacts match, which is only possible if $k_1 m_1 > k_2 m_2$ and $\omega_{c1} > \omega_{c2}$ or $k_1 m_1 < k_2 m_2$ and $\omega_{c1} < \omega_{c2}$. The intersection frequency ω_* is found equating $\Gamma_1(\omega_*) = \Gamma_2(\omega_*)$ as

$$\omega_*^2 = \begin{cases} 4 \frac{k_1 k_2}{m_1 m_2} \frac{(m_1 k_1 - m_2 k_2)}{k_1^2 - k_2^2} & \text{if } k_1 \neq k_2 \\ [0, \min(\omega_{c1}, \omega_{c2})] & \text{if } k_1 = k_2 \text{ and } m_1 = m_2 \\ \text{never} & \text{if } k_1 = k_2 \text{ and } m_1 \neq m_2 \end{cases}$$

The contacts do not match if $k_1 m_1 < k_2 m_2$ and $\omega_{c1} > \omega_{c2}$ or $k_1 m_1 > k_2 m_2$ and $\omega_{c1} < \omega_{c2}$ and transmission is constant if $\omega_{c1} = \omega_{c2}$.

Other OCI

Because the key to obtaining an OCI is the use of symmetric blocks, one can imagine that an abrupt interface between contacts built with different types of blocks is also an OCI. In fact, this is shown starting from a more general interface where two parameters m_0 and k_0 can be varied (Figure 6). Using the block concept to define the contacts and the impurities, phonon transmission is found to be

From this system, two single junction interfaces can be defined by setting k_i^{-1} (or m_i) to zero and letting m_0 (or k_0) vary. The cancelations in the denominator of Eq. (32) expose an OCI when $m_i = 0$ (or $k_i^{-1} = 0$), which is an upper bound of thermal conductance for any

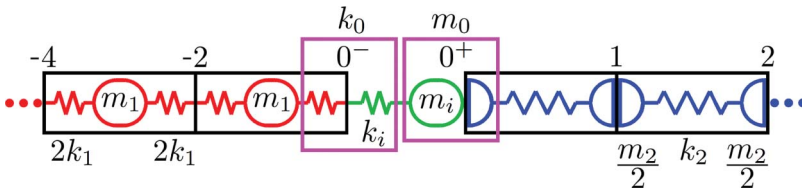


Figure 6 1D interface between dissimilar materials with an arbitrary bond k_0 ($\frac{1}{k_0} = \frac{1}{k_i} + \frac{1}{2k_1}$) and atom m_0 ($m_0 = m_i + \frac{m_2}{2}$) in between. An OCI between half-spring and half-mass contacts arises when $m_i = 0$ and $\frac{1}{k_i} = 0$. However, this OCI is an upper bound only for thermal conductance of systems in which m_0 vary arbitrarily and $\frac{1}{k_i} = 0$ or reciprocally. When k_0 and m_0 can vary together, interferences enter into the picture and the upper bound is lost (color figure available online).

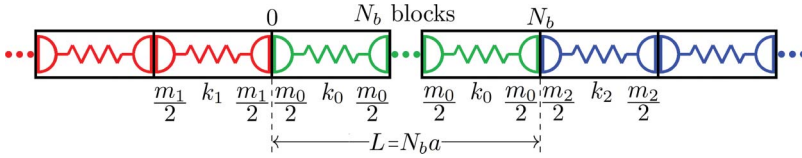


Figure 7 System consisting of two mediums sandwiching a third one characterized by the broadenings Γ_1 , Γ_2 , and Γ_0 , respectively. Similar to the antireflection coating condition, transmission is unity when $L = \lambda/4$ and $\Gamma_0 = \sqrt{\Gamma_1\Gamma_2}$ (color figure available online).

other choice of m_i (or k_i^{-1}). Similar to the cases in the last subsection, plotting Γ_1^{hs} and Γ_2^{hm} reflects some transmission characteristics (Figures 5c and 5d). If the system is studied as a whole and both impurities do not vanish, the transmission of the OCI is not necessarily an upper bound for every ω . This does not contradict the previous definition of OCI because the interface allows two parameters to vary.

Extrapolation Example: Beyond Single Interfaces

In the subsection on continuous and discrete limits we showed that OCIs generalize continuous interfaces to the discrete limit, which allows the extrapolation of known results between limits by changing interfaces with OCI and acoustic impedance Z with broadening Γ . This analogy may provide a way to endow phonon engineering with existing design criteria from other engineering fields. For instance, broadband filtering techniques from microwave engineering may be useful to engineer interfaces with maximum thermal conductance. As an example of the generalization, let us consider a system consisting of two mediums sandwiching a third one with impedances Z_1 , Z_2 , and Z_0 , respectively. Recall that reflection is eliminated when the coupling medium has length of a quarter wavelength and impedance $Z_0 = \sqrt{Z_1Z_2}$. Applying the extrapolation rules to the known solution [25], the system turns into Figure 7 and its transmission is given by (the result can also be obtained following the process in previous section)

$$T = \frac{4\frac{\Gamma_1}{\Gamma_2}}{\left(\frac{\Gamma_1}{\Gamma_2} + 1\right)^2 \cos^2(q_0L) + \left(\frac{\Gamma_1}{\Gamma_0} + \frac{\Gamma_0}{\Gamma_2}\right)^2 \sin^2(q_0L)}, \quad (33)$$

with Γ s defined according to the block choice in each particular region. Similar to the antireflection condition, transmission is unity when $L = \lambda/4$ and $\Gamma_0 = \sqrt{\Gamma_1\Gamma_2}$.

Unlike the impedance formalism; that is, Eq. (33) replacing Γ with Z —the broadening formalism (Eq. (33)) includes the effects of nonlinear dispersion and atomistic details. A comparison of the transmission predicted by both formalisms is shown in Figure 8. Note that as the frequency increases and the nonlinearity of the dispersion becomes important, the transmission functions separate from each other. Also note that different atomistic details at the interface, defined by our block choice, generate different transmission functions.

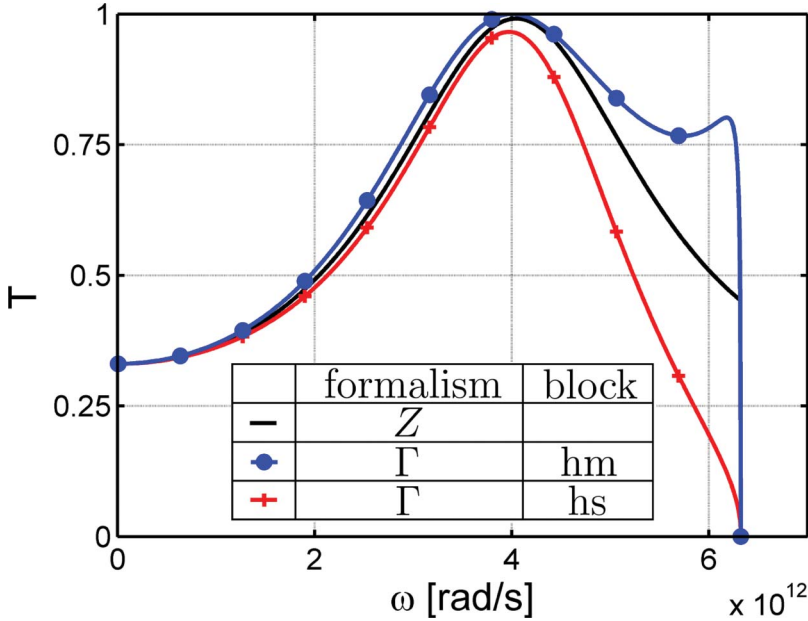


Figure 8 Comparison of the transmission function predicted by Eq. (33) (dotted line) and its counterpart with the long wavelength constraint; that is, Eq. (33) replacing Γ with Z (solid line). The system consists only of half-mass blocks (Figure 7) with $m_1 = 10^{-26}$ kg, $m_2 = 10^{-24}$ kg, $k_1 = k_2 = 10$ N/m, and $N_b = 3$. m_0 and k_0 were chosen to guarantee $T = 1$ at $\omega = 4 \times 10^{12}$ rad/s; that is, $m_0 = 1.1779 \times 10^{-25}$ kg and $k_0 = 7.0338$ N/m. The line with crosses represents the transmission of a system consisting only of half-spring blocks with the same parameters (color figure available online).

CONCLUSION

This article showed that the degree of mismatch at a single atom or bond interface depends on our ability to express the entire system solely in terms of building blocks on either side. Based on this concept, we argued that maximum thermal conductance occurs when the mass or bond junctions are the *arithmetic* or *harmonic* mean of their neighbors, respectively. Any deviation from those OCI adds an extra barrier for heat carriers, reducing the interfacial transmission and thermal conductance. We also showed that OCI and contact broadening (Γ) generalize continuous interfaces and acoustic impedance (Z) to the nonlinear phonon dispersion as well as the short-wavelength (atomic) limit. This generalization not only relates the continuum formalism with the discrete NEGF formalism but also provides a way to extrapolate previous results based on acoustic impedance to OCI. This may allow us to use existing techniques from other engineering fields to phonon engineering. For instance, broadband filtering techniques from microwave engineering may be useful to engineer interfaces with maximum thermal conductance.

REFERENCES

1. D.G. Cahill, W.K. Ford, K.E. Goodson, G.D. Mahan, A. Majumdar, H.J. Maris, R. Merlin, and S.R. Phillpot, Nanoscale Thermal Transport, *Journal of Applied Physics*, Vol. 93, pp. 793–818, 2003.

2. P.E. Hopkins, P.M. Norris, R.J. Stevens, T.E. Beechem, and S. Graham, Influence of Interfacial Mixing on Thermal Boundary Conductance Across a Chromium/Silicon Interface, *Journal of Heat Transfer*, Vol. 130, pp. 062402-1–062402-10, 2008.
3. P.E. Hopkins, L.M. Phinney, J.R. Serrano, and T.E. Beechem, Effects of Surface Roughness and Oxide Layer on the Thermal Boundary Conductance at Aluminum/Silicon Interfaces, *Physical Review B*, Vol. 82, pp. 085307–005307-5, 2010.
4. P.E. Hopkins, K. Hattar, T. Beechem, J.F. Ihlefeld, D.L. Medlin, and E.S. Piekos, Reduction in Thermal Boundary Conductance Due To Proton Implantation in Silicon and Sapphire, *Applied Physics Letters*, Vol. 98, pp. 231901-1–231901-3, 2011.
5. P.E. Hopkins, J.C. Duda, S.P. Clark, C.P. Hains, T.J. Rotter, L.M. Phinney, and G. Balakrishnan, Effect of Dislocation Density on Thermal Boundary Conductance Across GaSb/GaAs Interfaces, *Applied Physics Letters*, Vol. 98, pp. 161913-1–161913-3, 2011.
6. P.E. Hopkins, T. Beechem, J.C. Duda, K. Hattar, J.F. Ihlefeld, M.A. Rodriguez, and E.S. Piekos, Influence of Anisotropy on Thermal Boundary Conductance at Solid Interfaces, *Physical Review B*, Vol. 84, pp. 125408-1–125408-7, 2011.
7. W.-P. Hsieh, A.S. Lyons, E. Pop, P. Keblinski, and D.G. Cahill, Pressure Tuning of the Thermal Conductance of Weak Interfaces, *Physical Review B*, Vol. 84, pp. 184107-1–184107-5, 2011.
8. K.C. Collins, S. Chen, and G. Chen, Effects of Surface Chemistry on Thermal Conductance at Aluminum–Diamond Interfaces, *Applied Physics Letters*, Vol. 97, pp. 083102-1–083102-3, 2010.
9. J.C. Duda and P.E. Hopkins, Systematically Controlling Kapitza Conductance via Chemical Etching, *Applied Physics Letters*, Vol. 100, pp. 111602-1–111602-4, 2012.
10. M. Hu, P. Keblinski, and P.K. Schelling, Kapitza Conductance of Silicon\Char21{ }Amorphous Polyethylene Interfaces by Molecular Dynamics Simulations, *Physical Review B*, Vol. 79, pp. 104305-1–104305-7, 2009.
11. L. Hu, L. Zhang, M. Hu, J.-S. Wang, B. Li, and P. Keblinski, Phonon Interference at Self-Assembled Monolayer Interfaces: Molecular Dynamics Simulations, *Physical Review B*, Vol. 81, pp. 235427-1–235427-5, 2010.
12. Z.-Y. Ong and E. Pop, Molecular Dynamics Simulation of Thermal Boundary Conductance Between Carbon Nanotubes and SiO₂, *Physical Review B*, Vol. 81, pp. 155408-1–155408-7, 2010.
13. J.C. Duda, T.S. English, E.S. Piekos, W.A. Soffa, L.V. Zhigilei, and P.E. Hopkins, Implications of Cross-Species Interactions on the Temperature Dependence of Kapitza Conductance, *Physical Review B*, Vol. 84, pp. 193301-1–193301-4, 2011.
14. M. Shen, W.J. Evans, D. Cahill, and P. Keblinski, Bonding and Pressure-Tunable Interfacial Thermal Conductance, *Physical Review B*, Vol. 84, pp. 195432-1–195432-6, 2011.
15. Y. Wang and P. Keblinski, Role of Wetting and Nanoscale Roughness on Thermal Conductance at Liquid-Solid Interface, *Applied Physics Letters*, Vol. 99, pp. 073112-1–073112-4, 2011.
16. W.A. Little, The Transport of Heat Between Dissimilar Solids at Low Temperatures, *Canadian Journal of Physics*, Vol. 37, pp. 334–349, 1959.
17. E.T. Swartz and R.O. Pohl, Thermal Boundary Resistance, *Reviews of Modern Physics*, Vol. 61, pp. 605–668, 1989.
18. M.E. Lumpkin, W.M. Saslow, and W.M. Visscher, One-Dimensional Kapitza Conductance: Comparison of the Phonon Mismatch Theory with Computer Experiments, *Physical Review B*, Vol. 17, pp. 4295–4302, 1978.
19. R. Prasher, Acoustic Mismatch Model for Thermal Contact Resistance of van der Waals Contacts, *Applied Physics Letters*, Vol. 94, pp. 041905-1–041905-3, 2009.
20. L. Zhang, P. Keblinski, J.-S. Wang, and B. Li, Interfacial Thermal Transport in Atomic Junctions, *Physical Review B*, Vol. 83, pp. 064303-1–064303-9, 2011.
21. P.E. Hopkins, M. Baraket, E.V. Barnat, T.E. Beechem, S.P. Kearney, J.C. Duda, J.T. Robinson, and S.G. Walton, Manipulating Thermal Conductance at Metal–Graphene Contacts via Chemical Functionalization, *Nano Letters*, Vol. 12, pp. 590–595, 2012.

22. C.B. Saltonstall, C.A. Polanco, J.C. Duda, A.W. Ghosh, P.M. Norris, and P.E. Hopkins, Effect of Interface Adhesion and Impurity Mass on Phonon Transport at Atomic Junctions, *Journal of Applied Physics*, Vol. 113, pp. 013516-1–013516-8, 2013.
23. M.D. Losego, M.E. Grady, N.R. Sottos, D.G. Cahill, and P.V. Braun, Effects of Chemical Bonding on Heat Transport Across Interfaces, *Nature Materials*, Vol. 11, pp. 502–506, 2012.
24. S. Datta, *Quantum Transport: Atom to Transistor*, 2nd ed., New York, Cambridge University Press, 2005.
25. H.J. Pain, *The Physics of Vibrations and Waves*, 2nd ed., UK, Wiley, 1976.
26. P.E. Hopkins, P.M. Norris, M.S. Tsegaye, and A.W. Ghosh, Extracting Phonon Thermal Conductance Across Atomic Junctions: Nonequilibrium Green's Function Approach Compared To Semiclassical Methods, *Journal of Applied Physics*, Vol. 106, pp. 063503-1–063503-10, 2009.
27. N. Mingo and L. Yang, Phonon Transport in Nanowires Coated With an Amorphous Material: An Atomistic Green's Function Approach, *Physical Review B*, Vol. 68, pp. 245406-1–245406-12, 2003.
28. W. Zhang, T.S. Fisher, and N. Mingo, The Atomistic Green's Function Method: An Efficient Simulation Approach for Nanoscale Phonon Transport, *Numerical Heat Transfer, Part B*, Vol. 51, pp. 333–349, 2007.
29. J.-S. Wang, J. Wang, and J. T. Lü, Quantum Thermal Transport in Nanostructures, *The European Physical Journal B - Condensed Matter and Complex Systems*, Vol. 62, pp. 381–404, 2008.
30. N.W. Ashcroft and D.N. Mermin, *Solid State Physics*, 1st ed., Thomson Learning, Toronto, ON, Canada, 1976.